This article has been accepted for publication in a future issue of this journal, but has not been fully edited. Content may change prior to final publication. Citation information: DOI 10.1109/ACCESS.2020.3006985, IEEE Access

IEEE Access
Multidisciplinary | Rapid Review | Open Access Journal

Date of publication xxxx 00, 0000, date of current version xxxx 00, 0000.

*Digital Object Identifier 10.1109/ACCESS.2020.DOI*

# PDMS-FBG Based Fiber Optic System for Traffic Monitoring in Urban Areas

**M. FAJKUS[1], M. FRIDRICH[1], J. NEDOMA[1], R. KAHANKOVA[2], R. MARTINEK[2], E. BEDNAR[1], J. KOLARIK[2]**

[1]Department of Telecommunications, Faculty of Electrical Engineering and Computer Science, VŠB–Technical University of Ostrava, 708 00 Ostrava, Czech Republic
[2]Department of Cybernetics and Biomedical Engineering, Faculty of Electrical Engineering and Computer Science, VŠB–Technical University of Ostrava, 708 00 Ostrava, Czech Republic

Corresponding author: M. Fajkus (e-mail: marcel.fajkus@vsb.cz).

This article was supported by the Ministry of Education of the Czech Republic (Project No. SP2019/85). This article was also supported by the Ministry of Industry and Trade of the Czech Republic within the project No. FV10396. It was also supported by the European Regional Development Fund in the Research Centre of Advanced Mechatronic Systems project, project number CZ.02.1.01/0.0/0.0/16_019/0000867 within the Operational Programme Research, Development and Education. This work was supported by the European Regional Development Fund in Research Platform focused on Industry 4.0 and Robotics in Ostrava project, CZ.02.1.01/0.0/0.0/17_049/0008425 within the Operational Programme Research, Development and Education.

**ABSTRACT** This article introduces fiber Bragg grating (FBG) system for monitoring selected traffic flow parameters in urban areas. The system is able to monitor traffic density or speed of cars driving in single lane. The proposed system consists of five Bragg gratings encapsulated in Polydimethylsiloxane polymer and is characterized by easy and inexpensive installation in the milled upper layer of the road covered with an asphalt mixture. The results of first operational tests presented in this study include 3978 passing vehicles of various specifications. The system's vehicle detection success rate is 99.62%. And further, a mean absolute error 1.35 kph and a relative error 2.62% when measuring vehicle speed.

**INDEX TERMS** Fiber Bragg grating, PDMS-FBG sensor, Polydimethylsiloxane, road traffic monitoring, speed measurement.

## I. INTRODUCTION

Traffic sensors are devices that provide input data for traffic management systems. These sensors are installed primarily on and above the roadway or within the road surface. The basic information and traffic parameters provided by the sensors include vehicle speed, vehicle classification, wheelbase and number of axles, vehicle weight, axle load of the road, stopped vehicle detection, lane or direction change detection and traffic density, which indicates the quality of traffic flow. The traffic sensors are primarily divided into two basic groups, intrusive and non-intrusive (i.e. destructive or non-destructive to the road and its surroundings).

### A. STATE-OF-THE-ART SENSORS

The conventional traffic sensors include inductive loops [1], [2] and magnetic field sensors [3]. These are among the most commonly used sensors for their simplicity and reliability. On the other hand, they also have some disadvantages such as limited usage in reinforced concrete structures, higher costs associated with their installation in the road structures and the susceptibility to breakage due to heavy traffic.

Pneumatic sensors represent a portable technology with very easy installation. The principle of their operation is based on measuring the change in pressure in a pneumatic road tube [4], [5]. The drawback of the technology is that standing or slow-moving vehicles cannot be easily identified which causes inaccurate axle counts at higher traffic intensities. Moreover, this type of sensor is not used in adverse weather conditions, such as snow or rain.

Piezoelectric sensors [6]–[8] work on the principle of compression of a measuring probe placed in a milled in longitudinal groove. The voltage generated by the sensor is proportional to the force or weight (wheels or axles) of the passing car.

Microwave motion sensors [9], [10] uses electro-magnetic radiation; the vehicle speed is determined using micro-waves reflected back to the receiver based on the Doppler effect. The disadvantage of these sensors is their susceptibility to electromagnetic interference, radio waves are reflected from metal parts of car body and other obstacles, such as barriers,



This work is licensed under a Creative Commons Attribution 4.0 License. For more information, see https://creativecommons.org/licenses/by/4.0/.

This article has been accepted for publication in a future issue of this journal, but has not been fully edited. Content may change prior to final publication. Citation information: DOI 10.1109/ACCESS.2020.3006985, IEEE Access



street lighting poles, iron or concrete structures.

The principle of operation of Closed Circuit Television (CCTV) technology is based on the digitization of a static image, where the passage of the vehicle changes the values of color and brightness. This technology is based on a set of one or more interconnected video cameras and a powerful computer for data processing and analysis. Using CCTV, it is also possible to register state license plates [11] and calculate the vehicle speed using the total distance travelled and the time taken from start to finish of selected section. CCTV technology is not affected by vehicle changing lanes, because the cameras monitor all lanes and are interconnected [12], [13].

### B. FIBER OPTIC AND OPTICAL SENSORS

Fiber optic and optical sensors have different principles of operation and offer several significant advantages, such as reliability, accuracy, high sensitivity, electromagnetic and chemical resistance or a wide operating temperature range. These sensors are used in many areas, such as automobile traffic monitoring.

Active infrared sensor gates work on the principle of transmitting and receiving an optical beam (laser or infrared, respectively) between the transmitter and receiver. [14], [15]. This kind of measurement is of a portable or stationary nature and is designed for speed and traffic density monitoring, or excessive trucks measurement.

Another type of sensors is based on microbending effect [16], where the attenuation of the optical fiber changes as the car passes. The fibers are stored in special protective housing and installed into the road structure. This type of sensors is rather experimental and is widely used in practice. In addition to micro-bending technologies, interferometric systems have also been used among the literature, mostly to count automobile axles [17], [18].

A special type of fiber optic sensors are Bragg gratings. To detect vehicle passage and measure vehicle speed, these sensors can be installed in the road itself (invasively) [19] or they can be placed on the road surface for short-term non-invasive use [20]. Weigh-in-Motion (WIM) sensors are other widely used sensors in traffic flow monitoring. This type of sensor is mainly based on Bragg gratings, which are installed in the road in various forms of encapsulation [21]. Portable pads based on Bragg grating are also being developed for weighing cars, but their use is limited by the maximum speed of the monitored cars [22]. In general, WIM are used in conjunction with other systems, so that the overall system can, in addition to the vehicle weight, provide information on speed, license plates, driver's appearance, vehicle dimensions, etc.

Finally, Rayleigh scattering based distributed acoustic sensing (DAS) has emerged as a powerful and rapidly adopted sensing technology in the recent years. The DAS technology evaluates Rayleigh scattering in the fiber optic cables, where acoustic activity generates acoustic energy that is absorbed by molecules in the fiber core. This causes a phase shift in backscattered light, which is detected by the evaluation unit and subsequently analyzed. The application of this technology in automobile traffic has been demonstrated in [23], [24], the authors state that it is possible to monitor more traffic parameters (such as vehicle detection, direction, speed) using a single optical fiber.

## II. FIBER BRAGG GRATINGS

Fiber-optic Bragg gratings (FBGs) are a rapidly evolving group of fiber-optic single-point sensors [25]. Bragg gratings are formed by a structure with periodic variation in the index of the fiber core. In this structure, the refractive index of the core $n_1$ alternates with an increased refractive index $n_3 = n_1 + \delta_n$, where $\delta_n$ is the induced refractive index which results from exposure of the photosensitive optical fiber to UV light. Fig. 1 shows the structure and the operational principle of the Bragg grating.

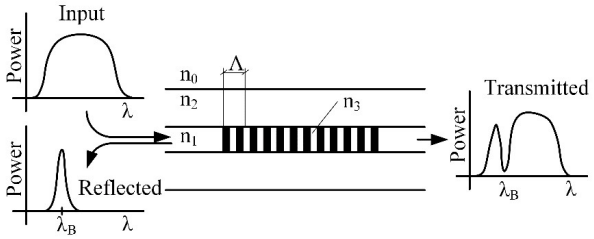


**FIGURE 1.** Operational principle and structure of the Bragg grating.

The structure of the Bragg grating reflects a narrow frequency band of the broadband light and transmits the others. The central part of the reflected spectrum is called the Bragg wavelength $\lambda_B$ and is given by:

$$\lambda_B = 2n_{eff}\Lambda, \tag{1}$$

where $n_{eff}$ is the effective refractive index of the grating in the fiber core $\Lambda$ is the grating period. Other wavelengths are transmitted without attenuation. The Bragg wavelength is the geometric and optical properties that change under the influence of mechanical and thermal stresses. The relation of the Bragg wavelength change, the relative deformation and temperature is expressed by the following relation:

$$\frac{\Delta\lambda_B}{\lambda_B} = k\epsilon + (\alpha_\Delta + \alpha_n)\,\Delta T \tag{2}$$

where $\Delta\lambda_B$ is Bragg wavelength shift, $k$ is deformation coefficient, $\varepsilon$ is deformation, $\alpha_\Lambda$ is the coefficient of thermal expansion, $\alpha_n$ is the thermo-optic coefficient and $\Delta T$ is change of temperature [26].

## III. DESIGN AND IMPLEMENTATION OF PDMS-FBG SENSOR

Road traffic monitoring using FBG sensors can be implemented using two approaches. In first, non intrusive approach, the sensors can be mounted overhead, to the side of the roadway or on the road surface non-invasively. The second, intrusive approach, requires the sensors being mounted



This work is licensed under a Creative Commons Attribution 4.0 License. For more information, see https://creativecommons.org/licenses/by/4.0/.

This article has been accepted for publication in a future issue of this journal, but has not been fully edited. Content may change prior to final publication. Citation information: DOI 10.1109/ACCESS.2020.3006985, IEEE Access



directly into the road structure (invasively). The non-invasive installation approach is only suitable for temporary use. This approach is characterized by a simpler implementation, but the life of these sensors is reduced, and it is also necessary to remove the sensors during winter road maintenance. The intrusive approach requires cutting into the road for installation and maintenance. Although this approach is more costly, its service life is longer and it is capable of continuous operation. This article describes an intrusive system that was invasively installed in the upper layer of the road structure.

Bragg gratings in a single-mode optical fiber with primary acrylate or polyimide protection have tensile strength but very susceptible to mechanical damage or breakage. For this reason, it is necessary to protect the optical fiber in sensory applications, especially when installed in the road, where the fibers must be invariant to chemical and thermal changes in concrete and also resistant to high pressure caused by from passing vehicles.

Different requirements are placed on the encapsulation of the Bragg grating. On the one hand, the sensor must be robust and resistant to the negative effects of the environment, but on the other hand it must have a sufficient sensitivity. Polymeric materials have been selected for encapsulating the Bragg gratings since they are sufficiently flexible for deformation measurements yet hard to break. Based on the initial tests and also previous experience [27]–[29]., the authors selected polydimethylsiloxane (PDMS), a polymeric two-component potting material.

PDMS is a non-toxic and non-flammable polymeric organosilicon compound that is resistant to chemicals, compressive stress, UV radiation. At the same time, it does not affect the function of FBG, see [30].

### A. PDMS-FBG SENSOR INSTALLATION TO ROADWAY

For the first phase of the experiments, we used a prototype of the PDMS-FBG sensor with dimensions of 60×30×7 mm. The sensor was made using single-mode optical fiber G.657.A with acrylate primary protection and Bragg grating (Bragg wavelength of 1548.388 nm, reflectance 93.3%, spectral width of 198 pm (full width at half maximum, FWHM)). The FBG fiber was placed in a mold printed on a 3D printer and subsequently encapsulated with PDMS Sylgard 184 polymer. SYLGARD 184 is a silicone elastomer kit which contains two chemicals polymeric base and a curing agent which cross-links with the polymeric matrix. Curing was carried out for 90 min at 80°C. Figure 2(a) shows a diagram illustrating the deployment of individual parts in the PDMS-FBG sensor, Figure 2(b) shows the sensor prototype. The fiber was protected by a PVC (Polyvinylchloride) tube with an outer dimension of 3 mm (PVC protection is visible in Fig. 3(a))

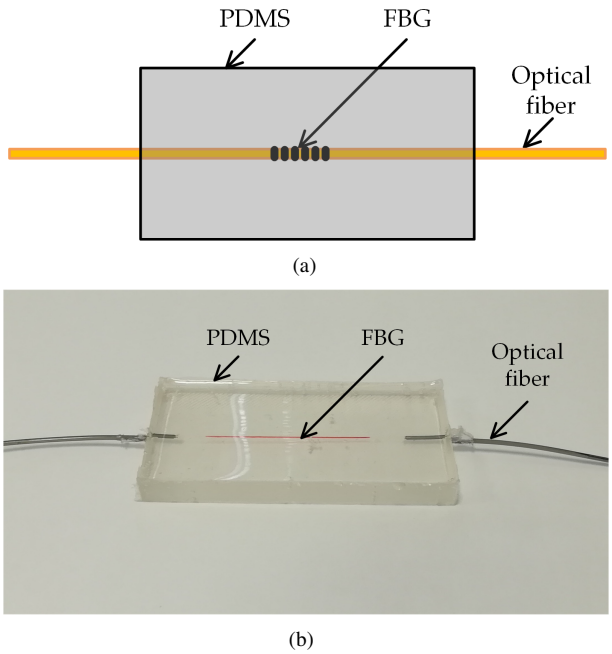


**FIGURE 2.** Illustration of PDMS-FBG sensor (a); Realized PDMS-FBG sensor prototype (b).

The PDMS-FBG sensor was embedded across in the monitored road surface, please see Fig. 3. In the first step, a longitudinal groove (2 m long, 10 mm wide,15 mm deep) was milled into the road. The PDMS-FBG sensor was placed in a part of the groove located 1 meter from the curb that was widened to the dimensions of about 80×120 mm, please see Fig. 3(a). In the second step, the groove with the sensor was filled with Biolast 2K asphalt (Nadler Strasentechnik, Barleben, Germany), see Fig. 3(b). The cold asphalt curing took place at an outdoors (temperature of 23 ± 1°C) and took 90 min.



This work is licensed under a Creative Commons Attribution 4.0 License. For more information, see https://creativecommons.org/licenses/by/4.0/.

This article has been accepted for publication in a future issue of this journal, but has not been fully edited. Content may change prior to final publication. Citation information: DOI 10.1109/ACCESS.2020.3006985, IEEE Access



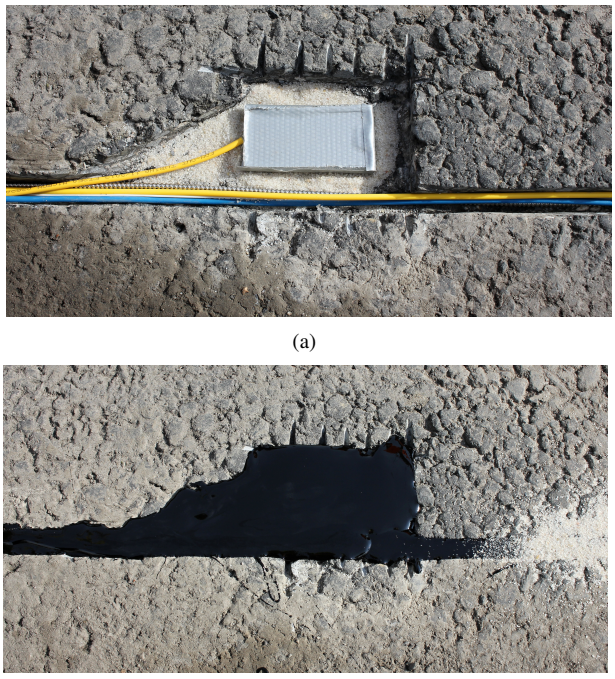

(a)

(b)

**FIGURE 3.** PDMS-FBG sensor placement in widened milled in groove (a); PDMS-FBG sensor covered with cold asphalt (b).

The effect of the curing process of the selected type of cold asphalt on the PDMS-FBG sensor Bragg wavelength is shown in Figure 4. A sharp increase of 411 pm (yellow area in Figure 4) related to asphalt-pouring is followed by a gradual decline of the wavelength (200 pm in 1.5 hours) associated with the curing process (blue area). The process of installing the sensor into the road surface caused an increase in the Bragg wavelength by about 190 pm. This small Bragg wavelength change during the installation and curing process does not lead to significant spectral requirements in the design of the sensor branch with five PDMS-FBG sensors described below. The asphalt curing process also does not affect the shape of the reflection spectrum, and thus the functionality of the PDMS-FBG sensor.

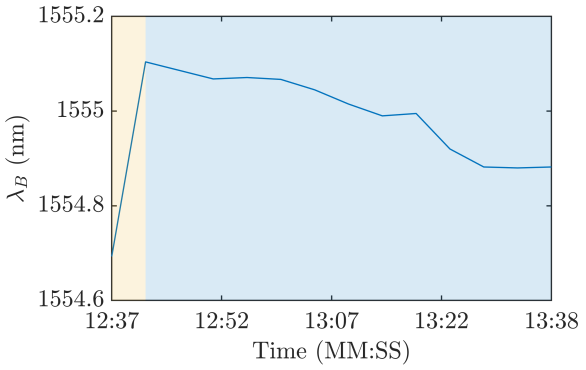


**FIGURE 4.** Effect of the curing process on PDMS-FBG sensor Bragg wavelength.

### B. PDMS-FBG SENSOR SPATIAL SENSITIVITY

Traffic density and speed monitoring is conditioned by accurate vehicle detection. Therefore, it is necessary to ensure the sensitivity of the sensor element to car passages along the entire width of the road lane (i.e. width of approx. 3.2 m – which is an average width of the roads in the Czech cities). The designed PDMS-FBG sensor is a single-point sensor; to cover the entire lane it is necessary to use n PDMS-FBG sensors connected in series. To determine the optimal number of sensors needed, it is necessary to know the spatial sensitivity of the PDMS-FBG sensor.

The spatial sensitivity of the sensor was determined by analyzing the magnitude of the sensor's response to the axle of the vehicle passage at various distances from the PDMS-FBG sensor. For this purpose, a grid was drawn on the road on both sides of the sensor with a spatial resolution of 5 cm (see Fig. 5). Subsequently, a test was carried out based on 642 passages of vehicles with various specifications (605 cars, 31 cars with a trailer, 6 trucks). The distance between the axle and the sensor was then determined for each vehicle using a video recording.

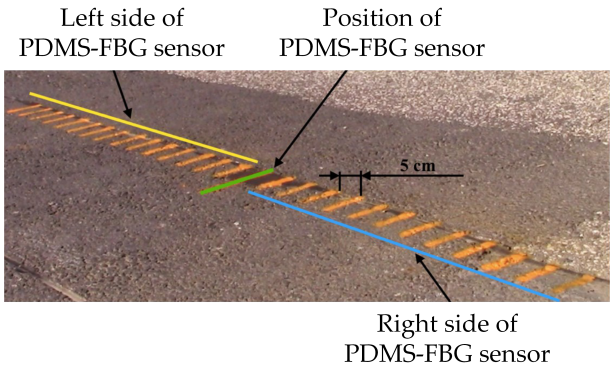


**FIGURE 5.** Grid marking PDMS-FBG position for spatial sensitivity analysis.

Figure 6 shows the responses of PDMS-FBG sensor to vehicle passage depending on the axle distance of the vehicle from the sensor. The axle passes directly via the PDMS-FBG sensor correspond to the highest response, which corresponds to an absolute value of 600 $\mu$m. As the crossing distance increases, the response decreases; for example, at a distance of 30 cm, absolute value of the response is 20 pm. This is the value that can be certainly detected by the evaluation unit since the minimum resolution is 1 pm. Based on this analysis, the maximum distance between PDMS-FBG sensors was set as 60 cm, i.e. the system is able to detect axle that passes between two sensors 60 cm apart.



This work is licensed under a Creative Commons Attribution 4.0 License. For more information, see https://creativecommons.org/licenses/by/4.0/.

This article has been accepted for publication in a future issue of this journal, but has not been fully edited. Content may change prior to final publication. Citation information: DOI 10.1109/ACCESS.2020.3006985, IEEE Access



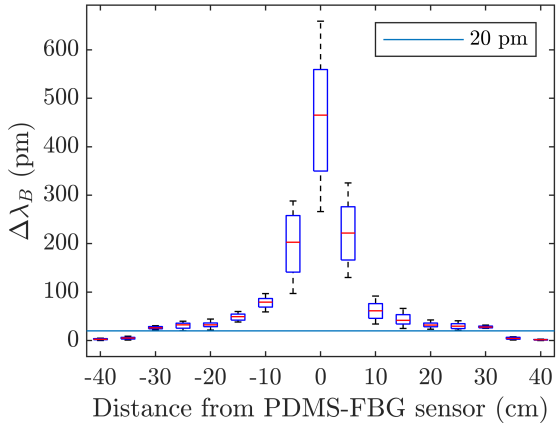


**FIGURE 6.** Effect of the distance between the sensor and the axle on PDMS-FBG sensor response.

### C. DESIGN AND IMPLEMENTATION OF PDMS-FBG SENSOR-CHAIN FOR SINGLE-LINE TRAFFIC MONITORING

Based on the above analysis, the spatial sensitivity of the PDMS-FBG sensor for vehicle detection was defined as ±30 cm. To cover the entire width of the 3.2 m lane, a sensor-chain with five PDMS-FBG sensors was designed, see Figure 7.

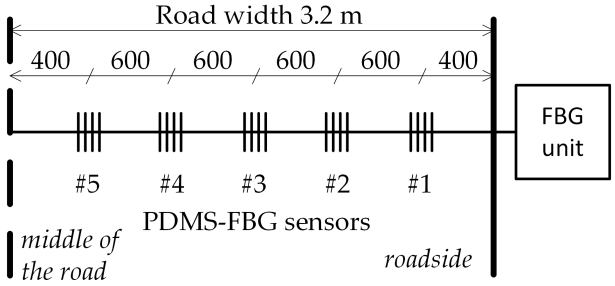


**FIGURE 7.** Single-line PDMS-FBG sensor deployment in the road with connection to the FBG evaluation unit.

In the next phase, it is also necessary to determine the spectral spacings of individual PDMS-FBG sensors. These spacings must be defined by the maximum possible sensor deflection caused by the car passage. Spacings must prevent overlapping of adjacent spectra, i.e. signal crosstalk.

In the pilot tests with a limited number of 642 passages, the maximum signal amplitude ranged from 583 pm to 631 pm. A spectral window must be assigned to each PDMS-FBG sensor and the individual spectral windows must not overlap. Individual PDMS-FBG sensors can only operate in their spectral windows, otherwise a measurement error, so-called first order crosstalk, can occur.

Although the pilot test performed involved vehicle passages of various specifications and weights, some margin is considered, which takes into account, for example, the passage of large goods vehicles (trucks), which may elicit an even greater response. Therefore, we selected the spectral windows size of 2 nm.

When modeling the sensory branch, it is necessary to consider other factors such as manufacturing tolerance of Bragg wavelength in FBG production, effect of Bragg grating encapsulation in PDMS polymer, effect of asphalt curing, uneven distribution of road temperature changes, etc. Based on analysis [31], which beyond the scope of this article, a 2 nm margin was defined. For this reason, 4 nm (2 nm for measuring and 2 nm for other factors described above) is available for each measuring channel.

Table 1 shows the Bragg wavelengths for individual phases, beginning with design of the sensory branch and culminating with the installation of the system in the roadway, and the spectral parameters of the measuring channels. In Table 1, 'Design' column includes the proposed Bragg wavelengths, whereas 'Used FBG' column shows the wavelengths of the FBGs produced. Moreover, the 'PDMS-FBG sensor' column includes the wavelengths of the implemented PDMS-FBG sensors and 'PDMS-FBG sensor in the road' column includes the wavelengths of PDMS-FBG sensors installed in the road after curing process. The last three columns include the maximum ($\lambda_{max}$) and minimum ($\lambda_{min}$) wavelengths defining the spectral window and its width.

Figure 8 illustrates the spectral distribution of the sensory branch. The Bragg wavelength is given for each reflection spectrum, and the width for each spectral window is shown in the lower part of the graph. Since the response to vehicle passage may be bipolar (positive and negative peaks, see Fig. 9), the spectral windows are defined to be symmetrical around the Bragg wavelength.

The PDMS-FBG sensor-chain with five PDMS-FBG sensors covers 20 nm of spectral space. When using two measuring chains, which will not overlap spectrally, it is possible to implement a single-line speed measurement with a one evaluation unit. The first measuring system can use a spectral space from 1510 to 1530 nm, the second from 1530 to 1550 nm. If speed measurement is required in two lanes, additional (third and fourth) measuring chains can be used and cover the spectral space from 1550 to 1570 nm and from 1570 to 1590 nm, respectively. All 4 chains will require 80 nm spectral space, which can be evaluated by one FBG evaluation unit, which has a SLED (superluminescent diode) as a light source with a spectral width of at least 80 nm.



This work is licensed under a Creative Commons Attribution 4.0 License. For more information, see https://creativecommons.org/licenses/by/4.0/.

This article has been accepted for publication in a future issue of this journal, but has not been fully edited. Content may change prior to final publication. Citation information: DOI 10.1109/ACCESS.2020.3006985, IEEE Access



**TABLE 1.** Spectral parameters PDMS-FBG sensory branch.

| ID | $\lambda_B$ (nm) | | | | Measuring spectral window (nm) | | |
|---|---|---|---|---|---|---|---|
| | Design | Used FBG | PDMS-FBG sensor | PDMS-FBG sensor in the road | $\lambda_{min}$ | $\lambda_{max}$ | Width |
| 1 | 1531 | 1531.243 | 1531.605 | 1531.912 | 1530.000 | 1533.749 | 3.75 |
| 2 | 1535 | 1535.031 | 1535.343 | 1535.585 | 1533.749 | 1537.393 | 3.64 |
| 3 | 1539 | 1539.113 | 1538.894 | 1539.201 | 1537.393 | 1541.582 | 4.19 |
| 4 | 1543 | 1542.989 | 1543.580 | 1543.963 | 1541.582 | 1546.076 | 4.49 |
| 5 | 1547 | 1547.203 | 1547.828 | 1548.188 | 1546.076 | 1550.000 | 3.92 |

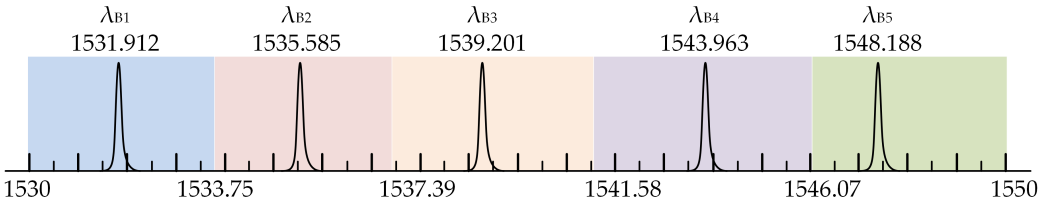


**FIGURE 8.** Operational principle and structure of the Bragg grating.

### *D. PDMS-FBG CHAIN SENSOR SIGNAL PROCESSING*

Figure 9(a) shows examples of raw signals from individual PDMS-FBG sensors (labeled as FBG1 – FBG5). The time window of 0.8 s shows a sample corresponding to the car passage at the speed of 53.74 kph. The response of individual PDMS-FBG sensors depends on the distance of the wheel from the measuring probe, vehicle (axle) weight, speed, etc. The individual sensors and the asphalt have a certain degree of flexibility; each passage is thus manifested by a positive peak followed by negative one, which is caused by the sensor stress release. The signal contains a low-frequency component corresponding to the memory effect and relaxation of the PDMS-FBG sensor and temperature change. These unwanted components are removed by a 4-order Butterworth high-pass filter with a cut-off frequency of 0.2 Hz. The filtered signal is shown in Figure 9(b).

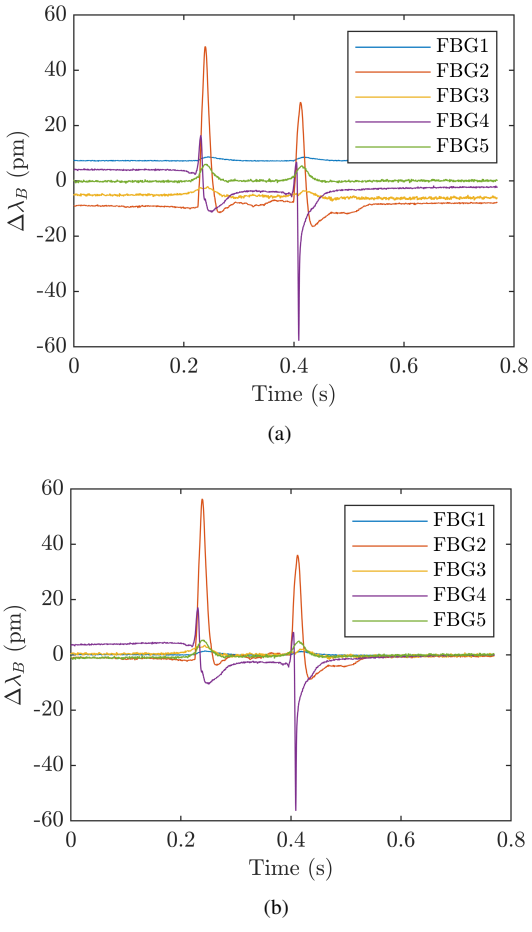


**FIGURE 9.** Example of system response to car passage at a speed of 53.74 kph; a) raw data from the PDMS-FBG chain sensor; (b) signals pre processed using a high-pass filter.



This work is licensed under a Creative Commons Attribution 4.0 License. For more information, see https://creativecommons.org/licenses/by/4.0/.

This article has been accepted for publication in a future issue of this journal, but has not been fully edited. Content may change prior to final publication. Citation information: DOI 10.1109/ACCESS.2020.3006985, IEEE Access



The PDMS-FBG chain sensor has been designed so that each axle is detected even if the passage takes place between two adjacent PDMS-FBG sensors. As a result, each passage stresses at least two sensors (unless the axle passes between the curb and the first sensor). When considering the axle load on several sensors, it is possible to sum signals from five PDMS-FBG sensors and obtain a more distinctive sum signal for vehicle passage detection. The individual responses of FBG sensors are typically manifested by a positive leading edge with a peak followed by a negative drop, caused by the elasticity of the PDMS material and asphalt at the moment of release of the axle load on the sensor branch. For this reason, only the positive parts of the response are taken into account in the signal processing.

Figure 10 shows the sum of the positive parts of the filtered signals from 5 sensors. The evaluation unit sampling frequency 1000 samples/s was selected as minimum sampling frequency that ensures reliable detection of individual axles at speeds in normal city traffic. This fact along with fast responses of the PDMS-FBG chain sensor allows us to differentiate the individual passing axles, please see Fig. 10. The above signal processing procedure has been applied to all data presented in this publication.

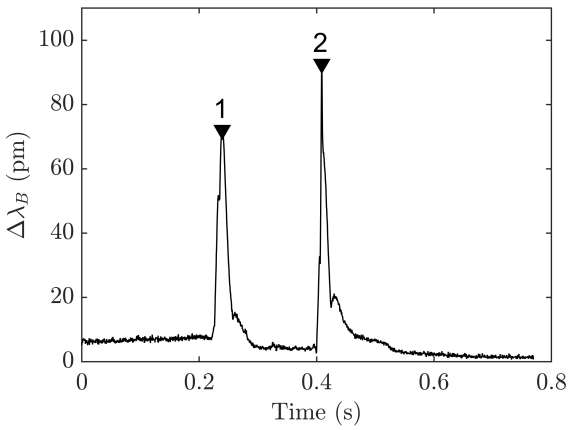


**FIGURE 10.** Sum signal corresponding to the car passage at 53.74 kph.

Figure 11 shows an example of a direct detection of 33 passing vehicles of various parameters. These vehicles' speed ranged from 32 to 87 kph with an overall response ranging from 33.36 to 339.55 pm.

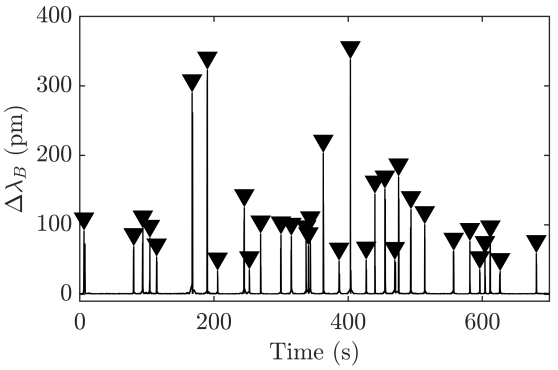


**FIGURE 11.** Example of detection of 33 cars with 100% accuracy.

Table 2 shows the responses of the PDMS-FBG sensors and the sum signal for 3 selected passes of the same car. The first passage was realized in the middle part of the lane (Fig. 12(a)). The design of the sensor branch allows these passages to be detected with all PDMS-FBG sensors. The second crossing was carried out in the middle of the road, and therefore the PDMS-FBG sensor close to the curb did not show any response (Fig. 12(b)). Similarly during the third passage, the sensor located closest to the center of the road did not detect the crossing of the car at the roadside (Fig. 12(c)).

**TABLE 2.** PMDS-FBG response to selected car passages

| Passage | FBG1 (pm) | FBG2 (pm) | FBG3 (pm) | FBG4 (pm) | FBG5 (pm) | Sum (pm) |
|---|---|---|---|---|---|---|
| 1 | 18.2 | 130.1 | 4.5 | 123.2 | 13.8 | 289.8 |
| 2 | - | 16.5 | 78.3 | 25.1 | 236.9 | 356.8 |
| 3 | 2.1 | 85.3 | 33.8 | 6.2 | - | 231.4 |



This work is licensed under a Creative Commons Attribution 4.0 License. For more information, see https://creativecommons.org/licenses/by/4.0/.

This article has been accepted for publication in a future issue of this journal, but has not been fully edited. Content may change prior to final publication. Citation information: DOI 10.1109/ACCESS.2020.3006985, IEEE Access



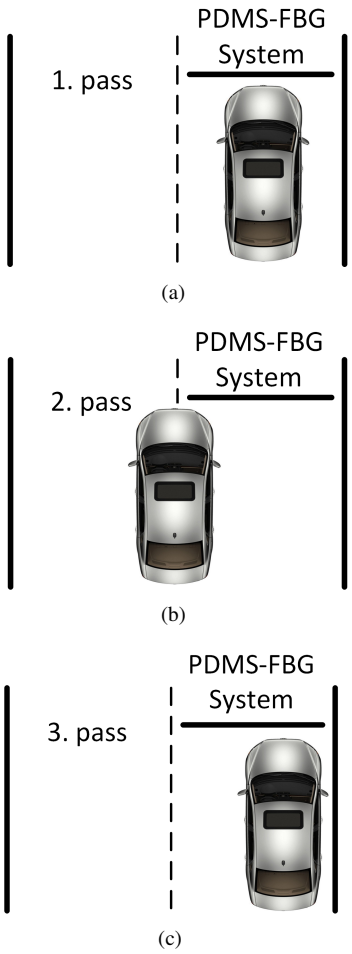


**FIGURE 12.** Display of selected car passages in various parts of the road (a) middle part of the lane; (b) middle of the road; (c) at the roadside.

The response of individual PDMS-FBG sensors to car crossings is illustrated in Figure 13. The blue bar represents the response of the PDMS-FBG sensor located at the roadside, the green bar corresponds to the PDMS-FBG sensor located in the middle of the road.

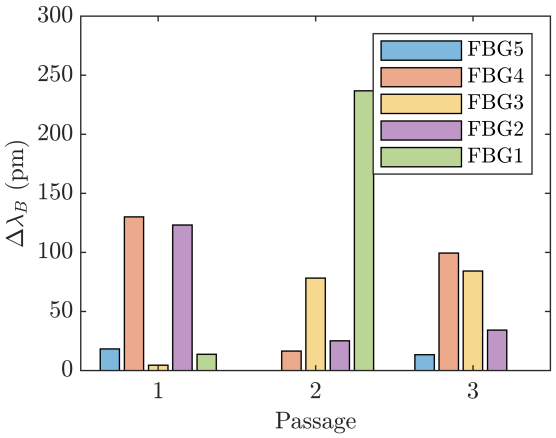


**FIGURE 13.** PDMS-FBG sensors responses on three crossings of the same car.

## IV. LONG-TERM MEASUREMENT AND EXPERIMENTAL VERIFICATION IN REAL OPERATION

This chapter describes and summarizes the results of the long-term traffic density and vehicle speed monitoring. The proposed measuring system using the PDMS-FBG chain sensor was tested in 18 all-day measurements taking place from January to November 2019 in city Ostrava (Part Vresina, GPS: 49°50'03.3"N 18°07'25.5"E). The measurements were carried out in various weather conditions (including adverse weather conditions such as rain, light snow or temperatures below freezing). Along with the PDMS-FBG system measurement, the team also took a video recording of the individual car passages, which provided following information: time of the passes, direction, type of vehicles. The reference speed of the vehicles was obtained using optical gates, see subchapter 4.2 for more details. As part of a long-term measurement, 16 motorcycle and 27 cyclist passes were detected, and were removed from the dataset.

### A. TRAFFIC DENSITY MONITORING

Figure 14 shows the results of the single-lane vehicle detection. The results display the traffic density for all 18 measuring days realized from January to November 2019.



This work is licensed under a Creative Commons Attribution 4.0 License. For more information, see https://creativecommons.org/licenses/by/4.0/.

This article has been accepted for publication in a future issue of this journal, but has not been fully edited. Content may change prior to final publication. Citation information: DOI 10.1109/ACCESS.2020.3006985, IEEE Access



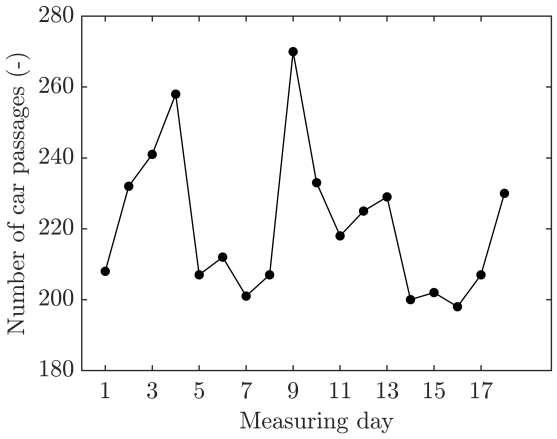


**FIGURE 14.** Results of traffic density monitoring.

During the measurement, a total of 3,978 vehicles (3,927 cars and 51 trucks) passed through the measuring area. The camera system captured all 3,978 vehicles while FBG measuring system was able to detect 3,963 vehicles. Summary of the detection accuracy is given in Table 3. The overall accuracy of vehicle detection using the proposed measuring system was 99.62%.

The measurements were analyzed and classified; the significant points were categorized as True Positive - TP, False Positive - FP or False Negative - FN) [32]. Based on that, the detection quality of the proposed system can be evaluated using parameters such as Sensitivity (SE), Accuracy (ACC), Positive Predictive Value (PPV), Harmonic mean of precision and sensitivity (F1) and False Negative Rate (FNR) [33].

$$SE = \frac{TP}{TP + FN}, \tag{3}$$

$$ACC = \frac{TP}{TP + FP + FN}, \tag{4}$$

$$PPV = \frac{TP}{TP + FP}, \tag{5}$$

$$F1 = 2\frac{PPV \cdot Se}{PPV + Se} = 2\frac{TP}{2TP + FP + FN}, \tag{6}$$

$$FNR = \frac{FN}{FN + TP}. \tag{7}$$

**TABLE 3.** Statistical evaluation of traffic density monitoring

| | FBG system | Reference Camera system |
|---|---|---|
| **N** | 3,978 | 3,978 |
| **TP** | 3,963 | 3,978 |
| **FP** | 6 | 0 |
| **FN** | 15 | 0 |
| **SE (%)** | 99.62 | 100 |
| **ACC (%)** | 99.47 | 100 |
| **PPV (%)** | 99.85 | 100 |
| **F1 (%)** | 99.74 | 100 |
| **FNR (%)** | 0.38 | 0 |

### B. VEHICLE SPEED MEASUREMENTS

Speed measurement requires placing at least two PDMS-FBG chain sensors in a given distance. The chain sensors were built into the road at a distance of 2 m from each other. For the reference speed measurement, a pair of optical gates was used. The gates were installed at the locations of individual chain sensors as displayed in Figure 15.

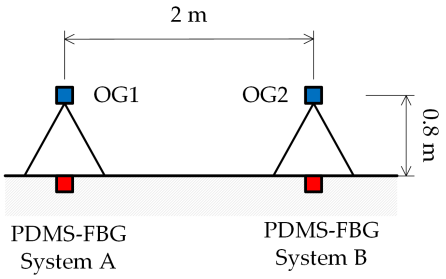


**FIGURE 15.** Basic layout diagram for measurement setup with PDMS-FBG chain sensors and optical gates for vehicle speed monitoring (PDMS-FBG chain systems are shown in red, optical gates (OG1 and OG2) in blue).

Figure 16 shows an example of vehicle speed measurement using signals from two PDMS-FBG chain systems corresponding to the vehicle passing at a speed of 63.33 kph. This reference was recorded using the optical gates. The speed can be calculated as $v = L/\Delta t$, where $L$ is the distance between the individual chain sensors (2 m) and $\Delta t$ is the time difference between the peaks corresponding to the passage of the first axle (respectively second axle) over PDMS-FBG A and PDMS-FBG B sensor system. The resulting speed for first and second axle is $v_{1axle} = 62.46$ kph and $v_{2axle} = 62.56$ kph, respectively. By averaging these two values, we obtain a more accurate estimate of the speed $v = 62.51$ kph. This way, we determined a speed measurement error of 0.82 kph with a relative error of 1.29% related to the actual speed of the passing car.



This work is licensed under a Creative Commons Attribution 4.0 License. For more information, see https://creativecommons.org/licenses/by/4.0/.

This article has been accepted for publication in a future issue of this journal, but has not been fully edited. Content may change prior to final publication. Citation information: DOI 10.1109/ACCESS.2020.3006985, IEEE Access



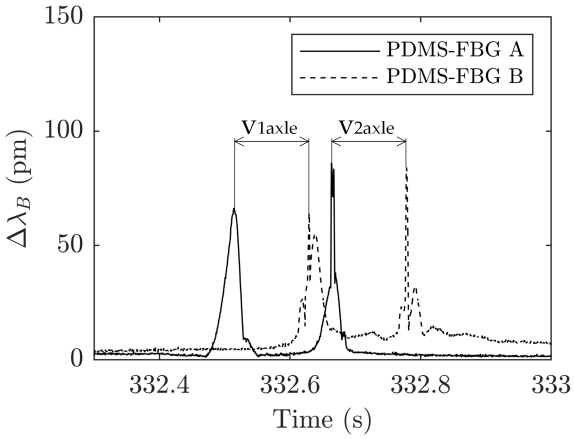


**FIGURE 16.** Example of vehicle speed measuring using two signals from PDMS-FBG A and PDMS-FBG B system corresponding to the passage of a car at a speed of 63.33 kph.

Figure 17(a) shows the real speeds of 3,963 vehicles obtained by the optical gates. The average speed of the passages was 50.93 kph, the lowest speed was 38.00 kph, and the maximum speed was 63.99 kph. The speed measurement error is shown in Fig. 17(b), and the relative error in Fig. 17(c).

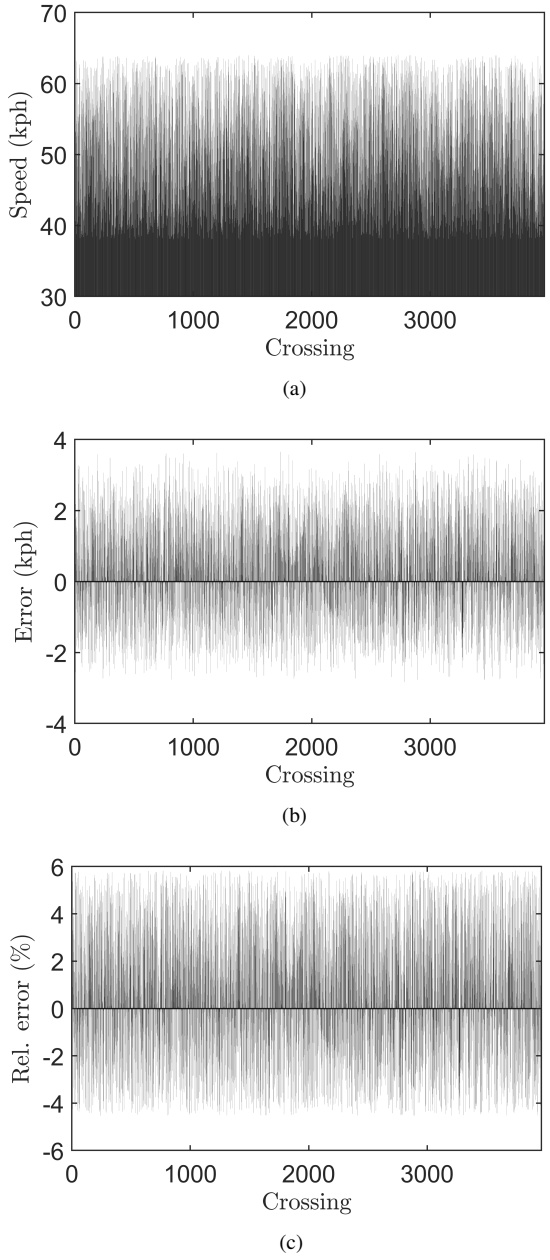


**FIGURE 17.** Example of speed measurement in 33 vehicles: (a) vehicle speed; (b) absolute error; (c) relative error (c).

Table 4 summarizes the long-term speed measurement accuracy. Mean absolute error of the FBG speed measurement was 1.35 kph (mean relative error 2.65%). Maximum absolute error reached 3.65 kph, this worst case occurred at the vehicle speed of 63.28 kph).



This work is licensed under a Creative Commons Attribution 4.0 License. For more information, see https://creativecommons.org/licenses/by/4.0/.

This article has been accepted for publication in a future issue of this journal, but has not been fully edited. Content may change prior to final publication. Citation information: DOI 10.1109/ACCESS.2020.3006985, IEEE Access



**TABLE 4.** Statistical evaluation of long-term speed measurement

| | Speed (kph) | Absolute error (kph) | Relative error (%) |
|---|---|---|---|
| **Min** | 38.00 | - | - |
| **Max** | 63.99 | 3.65 | 5.83 |
| **Mean** | **50.93** | **1.35** | **2.65** |

## V. CONCLUSION

The article presented the design, development and implementation of an optical fiber FBG system for monitoring selected traffic flow parameters in urban areas. The pilot study introduced herein included analysis of 3978 passing vehicles. The results revealed high accuracy of vehicle detection (99.62%) and speed measurements (mean absolute error 1.35 kph, mean relative error 2.65%). The advantages of the presented system include easy installation in the upper part of the road surface, possible connection to the existing dark (unused) fibers along city roads and implementation of remote evaluation within the SMART cities concept.

This pilot study presents the results a long-term research, in which 18 full-day measurements were performed from January to November 2019 in different weather conditions. Despite extensive research and development, there are still several issues and uncertainties that need to be addressed in follow-up research. This is primarily the effect of adverse weather conditions on the sensitivity and accuracy of the measurement and the overall life of the PDMS-FBG chain sensor in the roadway.

## REFERENCES

[1] X.-Y. Lu, P. Varaiya, R. Horowitz, Z. Guo, and J. Palen, "Estimating traffic speed with single inductive loop event data," *Transportation Research Record: Journal of the Transportation Research Board*, vol. 2308, no. 1, pp. 157–166, jan 2012.

[2] T. Cherrett, H. Bell, and M. McDonald, "Estimating vehicle speed using single inductive loop detectors," *Proceedings of the Institution of Civil Engineers - Transport*, vol. 147, no. 1, pp. 23–32, feb 2001.

[3] V. Markevicius, D. Navikas, M. Zilys, D. Andriukaitis, A. Valinevicius, and M. Cepenas, "Dynamic vehicle detection via the use of magnetic field sensors," *Sensors*, vol. 16, no. 1, p. 78, jan 2016.

[4] P. Zheng and M. Mike, "An investigation on the manual traffic count accuracy," *Procedia - Social and Behavioral Sciences*, vol. 43, pp. 226–231, 2012.

[5] P. T. McGowen and M. Sanderson, "Accuracy of pneumatic road tube counters," in *Institute of Transportation Engineers (ITE)*. Western District Annual Meeting, 2011, pp. 1–17.

[6] G. Guido, V. Gallelli, D. Rogano, and A. Vitale, "Evaluating the accuracy of vehicle tracking data obtained from unmanned aerial vehicles," *International Journal of Transportation Science and Technology*, vol. 5, no. 3, pp. 136–151, oct 2016.

[7] D. Xu, S. Huang, Q. Lei, and X. Cheng, "Preparation, properties and application research of piezoelectric traffic sensors," *Procedia Engineering*, vol. 27, pp. 269–280, 2012.

[8] S. Bhalla and S. Deb, "A cost-effective approach for trafic monitoring using piezo-tranducers," *Experimental Techniques*, vol. 35, no. 5, pp. 30–34, jul 2010.

[9] P. Heide, R. Schubert, V. Magori, and R. Schwarte, "A high performance multisensor system for precise vehicle ground speed measurement," *Microwave Journal*, vol. 39, no. 7, pp. 22–29, 1996.

[10] V. C. Nguyen, D. K. Dinh, V. A. Le, and V. D. Nguyen, "Length and speed detection using microwave motion sensor," in *2014 International Conference on Advanced Technologies for Communications (ATC 2014)*. IEEE, oct 2014, pp. 371–376.

[11] D. Zhang and J. He, "Super-resolution reconstruction of low-resolution vehicle plates: A comparative study and a new algorithm," in *2014 7th International Congress on Image and Signal Processing*. IEEE, oct 2014.

[12] H. A. Rahim, U. U. Sheikh, R. B. Ahmad, A. S. M. Zain, and W. N. F. W. Ariffin, "Vehicle speed detection using frame differencing for smart surveillance system," in *10th International Conference on Information Science, Signal Processing and their Applications (ISSPA 2010)*. IEEE, may 2010, pp. 630–633.

[13] C.-Y. Hsieh and Y.-S. Wang, "Traffic situation visualization based on video composition," *Computers & Graphics*, vol. 54, pp. 1–7, feb 2016.

[14] H. Ai and Y. Zheng, "Characterization of a traffic management system using pyroelectric infrared sensors," *Instrumentation Science & Technology*, vol. 43, no. 3, pp. 319–333, jan 2015.

[15] M. Rivas-Lopez, C. A. Gomez-Sanchez, J. Rivera-Castillo, O. Sergiyenko, W. Flores-Fuentes, J. C. Rodriguez-Quinonez, and P. Mayorga-Ortiz, "Vehicle detection using an infrared light emitter and a photodiode as visualization system," in *2015 IEEE 24th International Symposium on Industrial Electronics (ISIE)*. IEEE, jun 2015, pp. 972–975.

[16] P. Suopajaervi, R. Pennala, M. Heikkinen, P. Karioja, V. Lyori, R. A. Myllylae, S. M. Nissilae, H. K. Kopola, and H. Suni, "Fiber optic sensors for traffic monitoring applications," in *Smart Structures and Materials 1998: Smart Systems for Bridges, Structures, and Highways*, S. C. Liu, Ed. SPIE, jun 1998.

[17] D. Donlagic and M. Hanc, "Vehicle axle detector for roadways based on fiber optic interferometer," in *Smart Structures and Materials 2003: Smart Sensor Technology and Measurement Systems*, D. Inaudi and E. Udd, Eds. SPIE, jul 2003, pp. 317–321.

[18] ——, "A simple fiber-optic vehicle axle detector for roadways," *IEEE Transactions on Vehicular Technology*, vol. 52, no. 2, pp. 401–405, mar 2003.

[19] M. Kunzler, R. Edgar, E. Udd, T. Taylor, W. L. Schulz, W. Kunzler, and S. M. Soltesz, "Fiber grating traffic monitoring systems," in *Smart Structures and Materials 2002: Smart Systems for Bridges, Structures, and Highways*, S.-C. Liu and D. J. Pines, Eds., no. 4696. SPIE, jun 2002, pp. 238–243.

[20] M. Fridrich, M. Fajkus, P. Mec, J. Nedoma, M. Kostelansky, and E. Bednar, "Portable optical fiber bragg grating sensor for monitoring traffic density," *Applied Sciences*, vol. 9, no. 22, p. 4796, nov 2019.

[21] K. Wang, Z. Wei, B. Chen, and H.-L. Cui, "A fiber-optic weigh-in-motion sensor using fiber bragg gratings," in *Fiber Optic Sensor Technology and Applications IV*, vol. 6004. International Society for Optics and Photonics, 2005, p. 60040S.

[22] H. Zhang, Z. Wei, L. Fan, S. Yang, P. Wang, and H.-L. Cui, "A high speed, portable, multi-function, weigh-in-motion (wim) sensing system and a high performance optical fiber bragg grating (fbg) demodulator," in *Sensors and Smart Structures Technologies for Civil, Mechanical, and Aerospace Systems 2010*, vol. 7647. International Society for Optics and Photonics, 2010, p. 76473D.

[23] D. Hill, "Distributed acoustic sensing (DAS): Theory and applications," in *Frontiers in Optics 2015*. OSA, 2015.

[24] G. L. Duckworth, "Distributed sensing applications of rayleigh scattering in fiber optic cables," in *Imaging and Applied Optics*. OSA, 2013.

[25] K. Hill and G. Meltz, "Fiber bragg grating technology fundamentals and overview," *Journal of Lightwave Technology*, vol. 15, no. 8, pp. 1263–1276, 1997.

[26] A. Othonos, "Fiber bragg gratings," *Review of Scientific Instruments*, vol. 68, no. 12, pp. 4309–4341, dec 1997.

[27] M. Novak, J. Nedoma, M. Fajkus, J. Jargus, and V. Vasinek, "Analysis of optical properties of special fibers of polydimethylsiloxane (PDMS) depending on the different methods of mixing PDMS and curing agent," in *Micro-structured and Specialty Optical Fibres V*, K. Kalli, J. Kanka, A. Mendez, and P. Peterka, Eds., vol. 10232. SPIE, may 2017.

[28] J. Nedoma, M. Fajkus, P. Siska, R. Martinek, and V. Vasinek, "Non-invasive fiber optic probe encapsulated into PolyDiMethylSiloxane for measuring respiratory and heart rate of the human body," *Advances in Electrical and Electronic Engineering*, vol. 15, no. 1, mar 2017.

[29] M. Fajkus, J. Nedoma, R. Martinek, V. Vasinek, H. Nazeran, and P. Siska, "A non-invasive multichannel hybrid fiber-optic sensor system for vital sign monitoring," *Sensors*, vol. 17, no. 12, p. 111, jan 2017.

[30] J. Nedoma, M. Fajkus, L. Bednarek, J. Frnda, J. Zavadil, and V. Vasinek, "Encapsulation of FBG sensor into the PDMS and its effect on spectral



This work is licensed under a Creative Commons Attribution 4.0 License. For more information, see https://creativecommons.org/licenses/by/4.0/.

This article has been accepted for publication in a future issue of this journal, but has not been fully edited. Content may change prior to final publication. Citation information: DOI 10.1109/ACCESS.2020.3006985, IEEE Access



and temperature characteristics," *Advances in Electrical and Electronic Engineering*, vol. 14, no. 4, nov 2016.

[31] M. Fajkus, J. Nedoma, S. Kepak, L. Rapant, R. Martinek, L. Bednarek, M. Novak, and V. Vasinek, "Mathematical model of optimized design of multi-point sensoric measurement with bragg gratings using wavelength divison multiplex," vol. 9889, 2016, cited By 24.

[32] A. Unler and A. Murat, "A discrete particle swarm optimization method for feature selection in binary classification problems," *European Journal of Operational Research*, vol. 206, no. 3, pp. 528–539, nov 2010.

[33] R. Trevethan, "Sensitivity, specificity, and predictive values: Foundations, pliabilities, and pitfalls in research and practice," *Frontiers in Public Health*, vol. 5, nov 2017.

MARCEL FAJKUS was born in 1987 in in the Czech Republic. He works as assistant professor at the VSB-TUO Technical University of Ostrava since 2016. His current research interests include fiber Bragg sensors and distributed systems in traffic, civil engineering, and biomedical applications.

MICHAEL FRIDRICH was born in Trutnov, Czech Republic, in 1995. He received the bachelor's and master's degrees in information and communication technology from the VSB - Technical University of Ostrava, in 2017 and 2019, where he is currently studying for a Ph.D. During his doctoral studies, he focuses on fiber Bragg sensors and distributed systems in transportation, construction, and biomedical applications.

JAN NEDOMA was born in 1988 in the Czech Republic. In 2014 he received his Masters degree in Information and Communication Technology from VSB-Technical University of Ostrava. Since 2014 he has worked here as a Research Fellow. In 2017 he successfully defended his dissertation thesis and works as assistant professor at the VSB Technical University of Ostrava. His current research interests include fiber-optic sensors in traffic, civil engineering, and biomedical applications. He has more than 135 journal and conference articles (Author h-index: 9 without self-citations) in his research areas and 8 valid patents.

RADANA KAHANKOVA was born in 1991 in Opava, Czech Republic. She received her Master's and PhD degree at the VSB–Technical University of Ostrava, the Department of Cybernetics and Biomedical Engineering and in 2016 and 2019, respectively. Her current research is focused on improving the quality of electronic fetal monitoring and magnetic resonance imaging.

RADEK MARTINEK was born in 1984 in Czech Republic. In 2009 he received his Master's degree in Information and Communication Technology from VSB–Technical University of Ostrava. Since 2012 he has worked here as a Research Fellow. In 2014 he successfully defended his dissertation thesis titled 'The Use of Complex Adaptive Methods of Signal Processing for Refining the Diagnostic Quality of the Abdominal Fetal Electrocardiogram'. He has became an Associate Professor in Technical Cybernetics in 2017 after defending the habilitation thesis titled 'Design and Optimization of Adaptive Systems for Applications of Technical Cybernetics and Biomedical Engineering Based on Virtual Instrumentation'. He has worked as an Associate Professor at VSB– Technical University of Ostrava since 2017. His current research interests include: Digital Signal Processing (Linear and Adaptive Filtering, Soft Computing - Artificial Intelligence and Adaptive Fuzzy Systems, Non-Adaptive Methods, Biological Signal Processing, Digital Processing of Speech Signals); Wireless Communications (Software - Defined Radio); Power Quality Improvement. He has more than 200 journal and conference articles in his research areas.

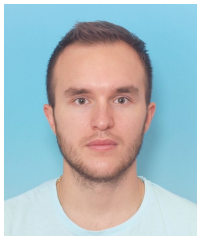

EMIL BEDNAR was born in Ilava, Slovakia, in 1995. He received the bachelor's and master's degrees in information technologies from the Department of Information and Communications Technologies, Faculty of Electrical Engineering and Computer Science, VSB - Technical University of Ostrava, in 2017 and 2019, where he is currently pursuing the Ph.D. degree. His current research interests include fiber-optic sensors predominantly in traffic and civil engineering.

JAKUB KOLARIK was born in Ostrava, Czech Republic, in 1992. He received the bachelor's degree from the Department of Cybernetics and Biomedical Engineering, VŠB–Technical University of Ostrava, in 2014, and the master's degree in control and information systems from the Department of Cybernetics and Biomedical Engineering. He is currently pursuing the Ph.D. degree in technical cybernetics.



This work is licensed under a Creative Commons Attribution 4.0 License. For more information, see https://creativecommons.org/licenses/by/4.0/.